Mass Transfer in Packed Beds with Two-Phase Flow

ARTICLE *in* INDUSTRIAL & ENGINEERING CHEMISTRY PROCESS DESIGN AND DEVELOPMENT · MAY 2002

DOI: 10.1021/i260056a021

3 AUTHORS, INCLUDING:

Janez Levec
University of Ljubljana
116 PUBLICATIONS **3,925** CITATIONS

tration. Since the reaction was found to have an apparent order of reaction near 0.6 and to be flow rate dependent, the reaction occurs in the intermediate region where both chemical kinetic and mass transfer effects are present. As mentioned above, however, chemical kinetics appears to be the more important resistance.

Conclusion

The reaction rate of activated carbon with steam can be represented by the steam concentration to the 0.58 power. The activation energy was found to be 63.6 kcal/g-mol. Although it appears that the dominant resistance is the reaction rate, external mass transfer does have some effect.

Nomenclature

C = concentration of water in vapor phase, g-mol/cm^3
F = water feed rate, g-mol/min
k = reaction rate constant
n = order of reaction
r = mol of carbon consumed/min-g of carbon
R = gas constant, 1.98 cal/g-mol °R
S = mol of water consumed/mol of carbon consumed
T = temperature of reaction, °R
v = gas flow rate, cm^3/min at reactor temperature and pressure
W = weight of carbon bed, g
X = fraction of water converted

Superscripts
° = inlet
f = outlet

Literature Cited

Abel, W. T., Holden, J. H., *U.S. Bur. Mines Rept. Invest.*, **No. 6000**, 1–22 (1962).
Battelle Memorial Institute, Columbus Laboratories, Columbus, Ohio, March 1970.
Derman, B. M., Rogailin, Farberov, I. L., *Akad. Nauk SSSR, Tr. Inst. Goryuchikh Iskopaemyhk*, (13), (1960).
Gadsby, J., Hinshelwood, C. N., Sykes, K. W., *Proc. Roy. Soc. London, Ser., A* **187**, 129–151 (1946).
Long, F. J., Sykes, K. W., *Proc. Roy. Soc. London, Ser. A*, **193**, 377–399 (1948).
Loven, A. W., *Chem. Eng. Progr.*, **69** (11), 56–62 (1973).
Malinauskas, A. P., *Nucl. Eng., Chem. Eng. Progr. Symp. Ser., Part XXI*, **66** (104), 81–93 (1970).
McCabe, W. L., Smith, J. C., "Unit Operations of Chemical Engineering, McGraw-Hill, New York, N.Y., 1967.
Pilcher, J. M., Walker, P. L., Jr., Wright, C. C., *Ind. Eng. Chem.*, **47** (9), 1742–1749 (1955).
Riede, B. E., Hanesian, D., *Ind. Eng. Chem., Process Des. Dev.*, **14**, 70–74 (1975).
Schchibrya, G. C., Morozov, N. M., Temkin, M. I., *Kinet. Katal.*, **6**, 1057 (1965).
Walker, P. L., Rusinko, F. Jr., Austin, L. G., *Catalysis*, **11**, 133–221 (1959).

Received for review February 10, 1975
Accepted June 30, 1975

This work was supported in part by funds provided by the U.S. Department of the Interior Office of Water Resources Research through the Institute of Water Resources, University of Connecticut, as authorized under the Water Resources Research Act of 1964, PL-83-379, as amended.

Mass Transfer in Packed Beds with Two-Phase Flow

S. Goto,[1] J. Levec,[2] and J. M. Smith*

University of California, Davis, California 95616

Mass transfer coefficients were measured at 25°C and 1 atm for cocurrent liquid (water) and gas flow in beds of small particles (0.054–0.29 cm) of napthalene and CuO·ZnO. The coefficients for transfer between particle and liquid are not greatly different for the three arrangements: upflow, downflow (trickle bed), or liquid full. At high gas rates and low liquid rates upflow gives somewhat higher transport rates, while trickle beds are favored over liquid-full operation at high liquid rates. Desorption of oxygen was measured to obtain liquid-to-gas coefficients k_La when mass transfer in the liquid phase controlled interphase transport. For downflow such coefficients were independent of gas flow rate, but in upflow k_La increased with gas rate. Upflow gave higher coefficients at high gas and liquid rates. Desorption of napthalene from water to air was employed to evaluate the gas-side coefficient in liquid-to-gas transfer for trickle-bed operation. The results showed a high sensitivity to gas flow rate and a modest sensitivity to liquid rate.

In three-phase reactors involving gas and liquid flow as well as the solid catalyst particles, interphase mass transfer resistances are likely to be more important than for the simpler fluid–solid catalytic system. For example, Goto and Smith (1975b) and Baldi et al. (1974), in studies of the oxidation of aqueous solutions of formic acid, found both gas–liquid and liquid–solid mass transfer resistances to be significant in trickle-bed operation, while the mass transfer resistance was negligible for liquid-full (no gas phase) operation. Therefore, reliable information for mass transfer coefficients is often needed for design of packed-bed reactors with gas and liquid flow. Further, such information may help in deciding whether to use a cocurrent upflow or downflow (trickle-bed) flow arrangement. The data reported here were obtained to help fulfill these needs by supplementing the available information, which is particularly meager for beds of small particles. In particular, measurements were made for upflow and downflow in the same apparatus in order to obtain a direct comparison for these two methods of operation.

Particle–liquid mass transfer coefficients were deter-

[1] On leave from University of Nagoya, Japan.
[2] On leave from University of Ljubljana, Yugoslavia.

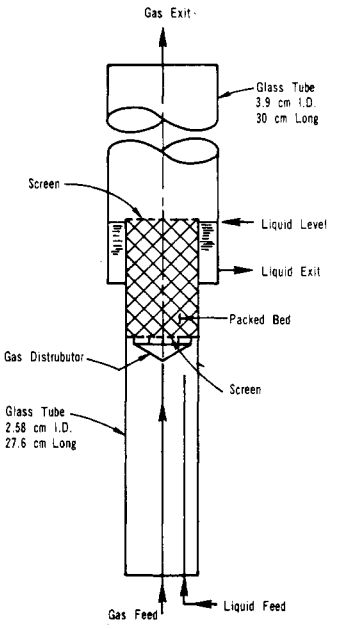

Figure 1. Bed arrangement for cocurrent upflow.

mined at 25°C and 1 atm pressure in a 2.58-cm i.d. glass tube packed with naphthalene particles (diameters of 0.0541, 0.108, or 0.241 cm) for cocurrent upflow and downflow of water and air. Liquid–gas coefficients were evaluated from data for the desorption of oxygen from water into nitrogen in beds packed with CuO·ZnO particles (diameter = 0.0541 or 0.291 cm). For these coefficients only upflow runs were made since downflow results for the same apparatus were available (Goto and Smith, 1975a). Such liquid–gas results are overall coefficients, and, in general, would represent the combined resistances to mass transfer in the gas and liquid phases. However, for slightly soluble oxygen, the data are a measure of the liquid phase resistance. Therefore, additional runs were made for the desorption of napthalene from water into air. For this system the Henry's law constant is low, corresponding to a very soluble gas and the resistance to mass transfer is predominately in the gas phase.

Snider and Perona (1974) measured combined gas–liquid and liquid–solid mass transport in cocurrent upflow and reported that the gas flow increased the transfer rate. Specchia et al. (1974) found liquid–gas mass transfer coefficients with cocurrent upflow were greater than those for downflow for the absorption of carbon dioxide in NaOH solutions and desorption of oxygen from water. Using the same chemical systems, Hirose et al. (1974) reported that the gas–liquid coefficients for downflow were greater than those for countercurrent flow. Saada (1972) measured gas–liquid coefficients for absorption of carbon dioxide into NaOH solutions for cocurrent upflow.

Particle-to-Liquid Mass Transfer

Figure 1 shows the packed bed arrangement for upflow and liquid-full operation. The upper part of the 2.58-cm i.d. glass tube containing the naphthalene particles was located concentrically inside a 3.9-cm i.d. tube to provide for separation of water liquid and air. The air was introduced through a distributor containing five capillary tubes (0.1 cm i.d. and 0.5 cm in length) equally spaced across the cross section of the 2.58-cm tube. Preliminary experiments showed that the 0.5-cm length of capillary provided enough flow resistance to ensure nearly equal flow of gas from each tube and an approximately uniform flux across the packed tube. The napthalene particles were held in place with

Table I. Physical Properties of Naphthalene Particles and Beds[a]

Size range	d_p, cm	ρ_p, g/cm^3	ρ_s, g/cm^3	Porosities ϵ_p	Porosities ϵ_B	a_t, cm^2/cm^3
7–9 mesh	0.241	1.04	1.15	0.096	0.433	14.1
14–16 mesh	0.108	1.04	1.15	0.096	0.437	31.3
28–32 mesh	0.0541	1.04	1.15	0.096	0.437	62.4

[a] Densities and porosities were determined from helium-pcynometer measurements. a_t was calculated by assuming spherical particles; i.e., $a_t = 6(1 - \epsilon_B)/d_p$. d_p, the equivalent spherical particle diameter, was taken as the average mesh size opening.

stainless steel screens (40 mesh) at the top and bottom of the bed, which was from 1.2 to 4.1 cm in length. For downflow operation the same 2.58-cm i.d. tube was used with the distributor, now used for liquid, placed at the top of the bed. The liquid and gas streams were separated at the bottom of the closed tube. Auxiliary apparatus included a feed reservoir for distilled water and gas cylinders with appropriate regulators for controlling the gas stream.

The same apparatus was used for gas–liquid mass transfer measurements. The feed reservoir was provided with a gas dispersion tube so that the distilled water could be saturated with oxygen.

For the particle–liquid runs the concentration of naphthalene in the effluent water stream was measured spectrophotometrically using a Beckman DK-2A spectrophotometer at a wavelength of 275 mμ. The so-measured concentration in a saturated solution at 25°C was 0.00360 g/(100 g of H_2O) in comparison with the reported solubility of 0.003–0.004 g/(100 g of H_2O) (Seidell, 1941). Because of the low solubility, the reduction in size of the naphthalene particles during a run was always less than 1.0%. Analysis of the air indicated that a negligible amount of naphthalene was in the exit gas stream.

The naphthalene particles were prepared by crushing and sieving pellets, retaining the 7 to 9, 14 to 16, and 28 to 32 mesh sizes. The physical properties of the three particle sizes and beds are given in Table I.

Particle-liquid mass transfer coefficients, $k_s a$, were calculated from the measured concentrations, $(C_{L,NA})_e$ of napthalene in the effluent stream and the mass balance

$$F_L dC_{L,NA} = k_s a(C^*_{L,NA} - C_{L,NA})S\, dz \qquad (1)$$

where $C^*_{L,NA}$ is the solubility of naphthalene in water at 25°C. This equation neglects axial dispersion, the effect of which may be estimated by predicting an axial diffusivity. As shown for downflow in the prior work (Goto and Smith, 1975a), this estimation indicated that the error in neglecting axial dispersion would be less than 10%, even for the short bed lengths employed. Integrating eq 1 and solving for $k_s a$ gives

$$k_s a = \frac{F_L}{S z_B} \ln\left[\frac{C^*_{L,NA} - (C_{L,NA})_f}{C^*_{L,NA} - (C_{L,NA})_e}\right] \qquad (2)$$

Mass transfer coefficients calculated from eq 2 for cocurrent downflow were nearly insensitive to the gas flow rate in the range of F_g = 0.0 to 4.0 cm^3/sec (25°C, 1 atm). For example, for 0.241-cm particles at F_L = 1.03 cm^3/sec, $k_s a$ varied but 6% over the entire range of F_g. Note that for F_g = 0.0 a gas phase is present in downflow operation. This is a different situation than for upflow, where for F_g = 0, no gas phase exists, and the column is liquid full. For cocurrent upflow, increasing the gas rate resulted in significant increases in $k_s a$. Results for both downflow (dotted lines) and upflow are shown in Figure 2.

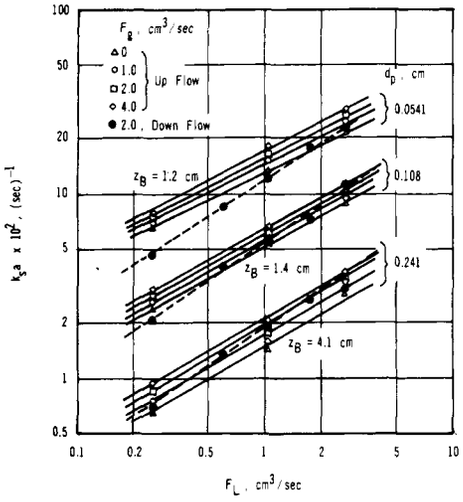

Figure 2. Particle-to-liquid mass transfer coefficients.

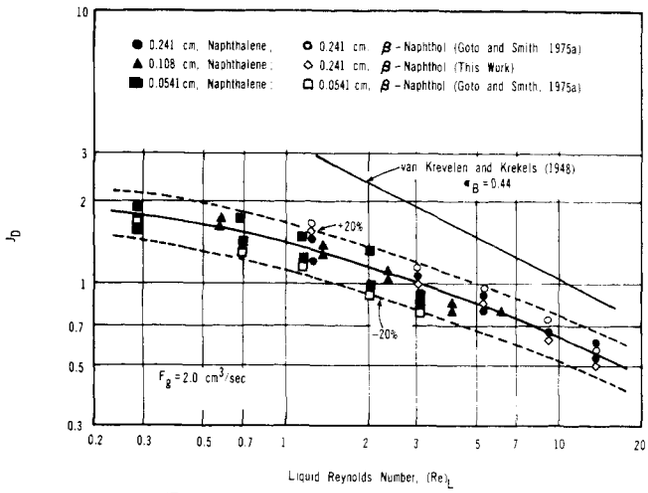

Figure 4. j_D vs. $(Re)_L$ for cocurrent downflow (trickle bed).

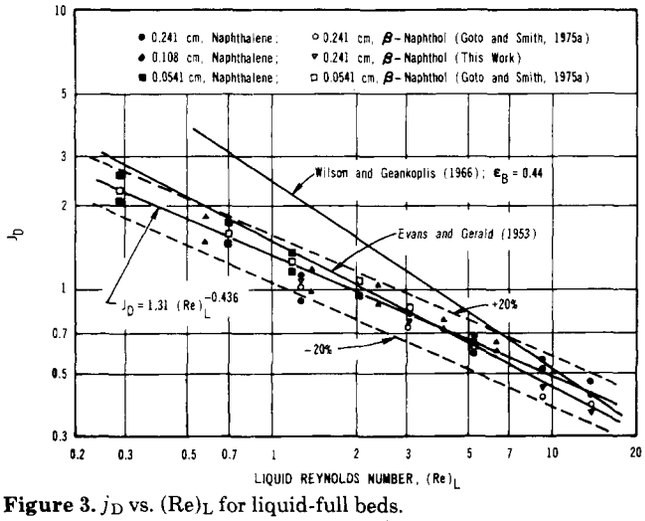

Figure 3. j_D vs. $(Re)_L$ for liquid-full beds.

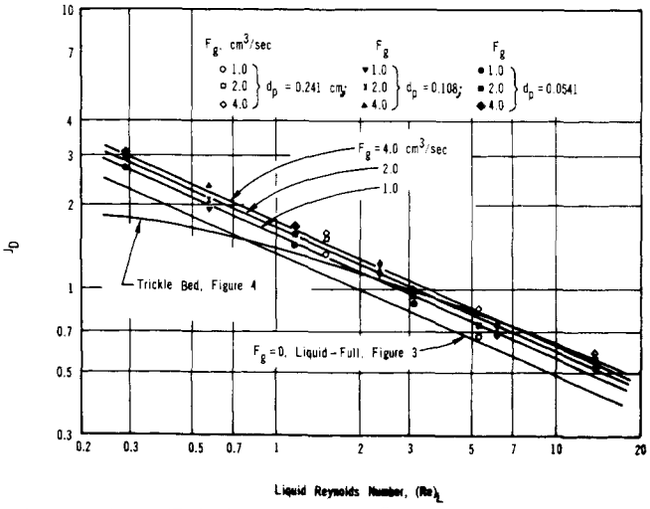

Figure 5. j_D vs. $(Re)_L$ for cocurrent upflow.

J_D factors were evaluated from the $k_s a$ values, using the expression

$$J_D = \frac{k_s a}{a_t}\left(\frac{1}{u_L}\right)\left(\frac{\mu_L}{\rho_L D}\right)^{2/3} \qquad (3)$$

where a_t is evaluated from d_p and ϵ_B as described in Table I. The molecular diffusivity of naphthalene in water at 25°C was estimated to be 0.708×10^{-5} cm²/sec from the Othmer and Thaker equation (Reid and Sherwood, 1966). Figures 3–5 present the naphthalene data for liquid-full, cocurrent downflow, and cocurrent upflow, plotted as J_D vs. Reynolds number. The previously determined (Goto and Smith, 1975a) results for transfer of β-naphthol, shown in Figures 3 and 4, agree well with the present data, thus providing a check of the reproducibility of the measurements. For liquid-full operation (Figure 3) there appears to be no effect of particle size, in the range studied, so that the results may be correlated by a single straight line

$$J_D = 1.31(Re_L)^{-0.436} \qquad (0.2 < Re_L < 20) \qquad (4)$$

Most of the results lie within ±20% of this line and agree with the measurements of Evans and Gerald (1953) for the transfer of benzoic acid particles to water (d_p = 0.05 to 0.2 cm). There is a deviation with respect to the results of Wilson and Geankoplis (1966) at low Reynolds numbers. These authors used spherical particles (d_p = 0.64 cm) and inert packed sections before and after the bed. These differences may explain the deviation.

For trickle-bed operation (Figure 4) the results for naphthalene and β-naphthol show no consistent difference and there is no effect of particle size. However, the data seem to suggest a convex curve rather than straight line. Such a flattening of the curve at low Reynolds numbers could be due to a decrease in effective surface area for mass transfer (a in eq 3). The correlation of Van Krevelen and Krekels (1948) does not agree with our results, but their correlation is based upon data outside (d_p = 0.29 to 1.4 cm) of the particle-size range studied here.

Figure 5 shows the data for cocurrent upflow and also includes the correlating (least-square-fit) curves for liquid-full and downflow operation from Figures 3 and 4. Comparison of these results indicates that J_D values are rather similar for the three flow arrangements. At high Reynolds numbers J_D for trickle beds is higher than for liquid-full operation, probably due to the greater linear liquid velocity when part of the void volume is occupied by gas. At low Reynolds numbers the effective mass transfer area for trickle-bed operation could explain the lower values for J_D. Figure 5 also shows that mass transfer is somewhat greater for upflow in comparison with either liquid full or downflow, particularly at high gas rates and low liquid Reynolds numbers.

Liquid-to-Gas Mass Transfer

Desorption of Oxygen. Liquid–gas mass transfer includes transport resistances in both phases. However, for

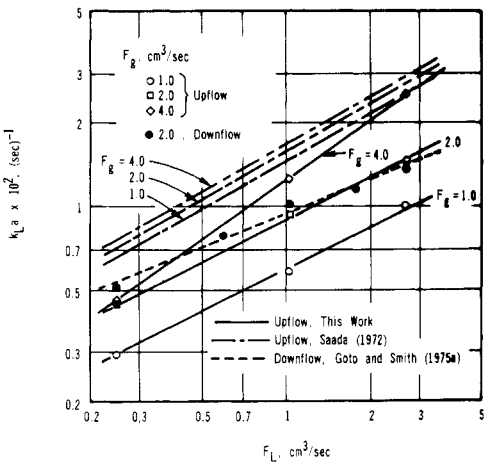

Figure 6. Mass transfer coefficients of oxygen from liquid to gas for d_p = 0.291 cm (liquid phase controlling).

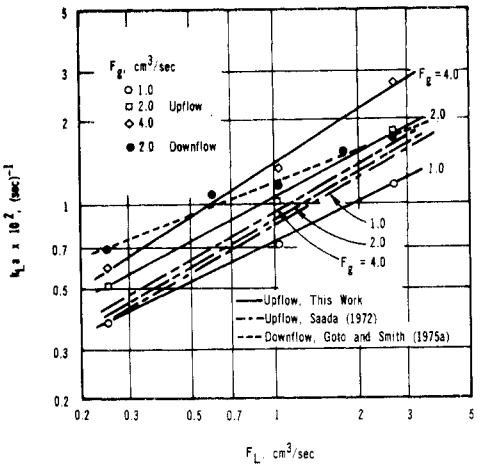

Figure 7. Mass transfer coefficients of oxygen from liquid to gas for d_p = 0.0541 cm (liquid phase controlling).

slightly soluble oxygen such interphase transfer is expected to be controlled by the liquid-phase resistance. The desorption measurements were made in the column shown in Figure 1. Pure nitrogen and distilled water saturated with pure oxygen were in upflow through the bed. The oxygen concentration in the effluent water was determined by first stripping the oxygen from the water in a packed, glass column with helium flow. Then the helium–oxygen mixture was analyzed in a chromatograph. Details and accuracy of the procedure are described by Baldi et al. (1974). Knowledge of the oxygen concentration in the feed and effluent water streams was sufficient, with available auxiliary information, to calculate the mass transfer coefficient, k_La, from liquid to gas. Similar results for downflow obtained in the same tube were already available (Goto and Smith, 1975a).

In liquid–gas systems there exists the possibility of mass transfer in the regions of the apparatus beyond the ends of the bed and before the liquid and gas streams are separated. The arrangement shown in Figure 1 was designed to minimize such end effects, but significant mass transfer did occur in these regions. The method of accounting for end effects consisted of removing the bed packing, raising the gas distributor and lower screen to just below the upper screen, and then measuring the concentration of oxygen in the effluent water. This concentration, $(C'_{L,O_2})_e$, was 24 to 59% less than the concentration in the feed. From measurements of both $(C'_{L,O_2})_e$ and $(C_{L,O_2})_e$ for each run it was possible to determine k_La for the bed. The procedure is to assume that mass transfer in the top and bottom end regions can be represented by $(k_La)_{top}$ and $(k_La)_{btm}$ which are different from k_La for the bed. Since the oxygen concentration in the gas stream is always very low, an error calculated to be less than 5% is introduced by neglecting C_{g,O_2}. Then, if axial dispersion is neglected, mass conservation equations for the two end sections and for the bed are

$$F_L dC_{L,O_2} = -(k_La)_{top}(C_{L,O_2} - 0)S\,dz \quad (5)$$

$$F_L dC_{L,O_2} = -(k_La)(C_{L,O_2} - 0)S\,dz \quad (6)$$

$$F_L dC_{L,O_2} = -(k_La)_{btm}(C_{L,O_2} - 0)S\,dz \quad (7)$$

Integration of these equations with the appropriate boundary conditions, and solution for k_La, yields

$$k_La = \frac{F_L}{Sz_B} \ln\left[\frac{(C_{L,O_2})_e'}{(C_{L,O_2})_e}\right] \quad (8)$$

A complete derivation of eq 8 is given by Goto and Smith (1975a).

The previous results for *downflow* and the present upflow k_La values are shown in Figures 6 and 7 for the two sizes of CuO·ZnO particles. The downflow data are given only for a gas rate of 2.0 cm³/sec (25°C, 1 atm) since over the range of F_g from 1.0 to 4.0 cm³/sec, k_La was essentially constant. This is evidence that k_La is controlled by transport in the liquid phase. The upflow data show a significant increase with increasing gas rate, probably due to increasing turbulence in the liquid phase as the gas rate is increased. Comparison for the two flow arrangements indicates that k_La is greater for upflow at high liquid and gas rates but less at the lowest flow rates. Further, the data show a mild increase in k_La with a decrease in particle size.

The "single-phase pore regime," as defined by Saada (1972), corresponds to our operating conditions. The values of k_La calculated from his correlation for upflow based upon beds of glass spheres (d_p = 0.05 to 0.2 cm) are also shown in Figures 6 and 7. For these calculations the molecular diffusivity of oxygen in water at 25°C was taken as 2.26×10^{-5} cm²/sec as calculated from the Othmer and Thaker equation (Reid and Sherwood, 1966). With respect to our data, Saada's results show less sensitivity to gas rate and the opposite variation with particle size.

Desorption of Napthalene. To complete the study of the liquid-to-gas case, it is desirable to evaluate mass transfer rates for a system where the resistance is predominantly in the gas phase. The desorption of naphthalene (dissolved in water) into air fits this situation. Assuming equilibrium at the gas–liquid interface and Henry's law, the relationship between the overall, K_La, and individual, k_La, k_ga, mass transfer coefficients may be written

$$\frac{1}{K_La} = \frac{1}{k_La} + \frac{1}{Hk_ga} \quad (9)$$

Since k_La and k_ga are the same order of magnitude (see Figures 6 and 10), the value of the Henry's law constant determines the relative importance of the transport resistances in the liquid and gas phases. For oxygen at 25°C, H is about 32.5 (Perry, 1963), where $H = C_g^*/C_L^*$. Hence, eq 9 shows that the measured K_La is approximately equal to k_La, a conclusion used in the earlier treatment of the oxygen desorption data. For naphthalene, H = 0.0168 at 25°C as calculated from the vapor pressure (0.0879 mm Hg, Washburn, 1929) and our measurement of the solubility in water, 2.81×10^{-7} mol/cm³. Then, $K_La = Hk_ga$, or $K_ga = k_ga$, approximately.

Downflow measurements were made for desorption of saturated solutions of naphthalene, in distilled water, into

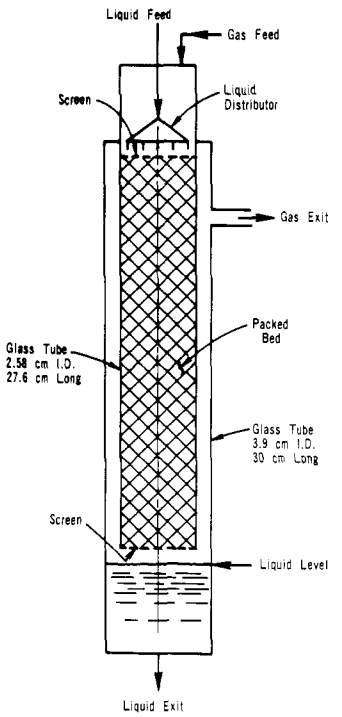

Figure 8. Bed arrangement for cocurrent downflow.

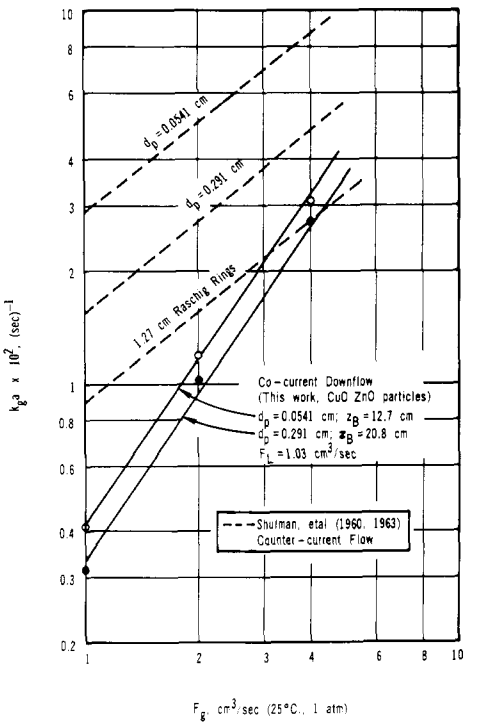

Figure 9. Liquid–gas mass transfer (gas phase controlling).

air. Since the change in concentration of naphthalene between feed and effluent water was too small to measure accurately, the naphthalene concentration in the exit air stream was determined. The determination was made in a Beckman DK-2A spectrophotometer using a 10-cm pathlength cell at 266-mμ wavelength where naphthalene has a large absorptivity. For the downflow arrangement the gas and liquid at the bottom of the bed were separated by surrounding the 2.58-cm tube with a larger tube up which the gas passed in the annular space on the way out of the apparatus, as shown in Figure 8.

Mass transfer in the end regions was important even though several less satisfactory phase-separation devices were tried before deciding on the arrangement shown in Figure 8. If $C^*_{g,NA}$ represents the concentration in the gas in equilibrium with water saturated with naphthalene, then $(Y'_{g,NA})_e$, where $(Y'_{g,NA})_e = (C'_{g,NA})_e/(C^*_{g,NA})$, varied from 0.18 to 0.54. The concentration $(C'_{g,NA})_e$ was measured by removing the packing and lowering the liquid distributor to just above the screen. The end effects were accounted for in the same manner as described for the oxygen desorption runs. The resulting expression used to calculate $k_g a$ is

$$k_g a = \frac{F_g}{S z_B} \ln \left[\frac{1 - (Y'_{g,NA})_e}{1 - (Y_{g,NA})_e} \right] \qquad (10)$$

The results for $k_g a$ show, as expected, a strong dependence on gas rate (Figure 9) and a minor dependence on liquid rate. Figure 10 shows all the data plotted versus F_L. The accuracy of these data is less than for the $k_s a$ measurements and the $k_L a$ data for oxygen desorption, as indicated by the increased scatter of the experimental points, for example, in Figure 10. We cannot explain the increase in $k_g a$ with gas rate to a power greater than unity, although the phenomenon was reproducible. End-effect corrections were large and perhaps less accurate, and this could affect the results. Also the range of F_g covered is relatively small, rendering uncertain conclusions about the influence of gas rate.

No published information was found for liquid–gas mass transfer in a cocurrent downflow system. Data and correla-

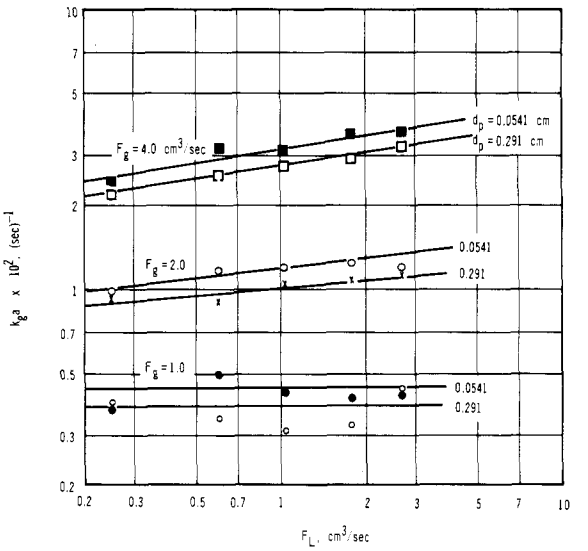

Figure 10. Effect of liquid flow rate on $k_g a$.

tions have been accumulated over many years for countercurrent flow with relatively large particle sizes (absorption-column data). Gas phase transfer coefficients evaluated from the Shulman (1960) correlation for transfer of naphthalene to air are included in Figure 9 for two cases. The lower line applies for 1.27 cm diameter Raschig rings; this is the smallest size for which the correlation is completely applicable. The upper lines were calculated for 0.0541-cm and 0.291-cm particles but using the data for 1.27-cm Raschig rings to estimate the effective mass-transfer area, a. Perhaps the approximate upper curves provide a more appropriate comparison with our cocurrent downflow data because the particle sizes are the same. However, any comparison must be suspect because the CuO-ZnO particle had small pores while the Shulman correlation is based upon hollow Raschig rings. The higher values for countercurrent

operation are reasonable in that turbulence in the gas phase is expected to be greater than for cocurrent downflow at the same flow rates.

Discussion

Depending on the values of the flow rates, different flow regimes occur in two-phase flow in packed beds. Our cocurrent downflow experiments were carried out with relatively low gas and liquid velocities, u_g = 0–0.77 cm/sec and u_L = 0.048–0.51 cm/sec. Weekman and Myers (1964) evaluated the boundaries of three flow regimes, and according to their work the data reported here fall in the gas-continuous regime. This agrees with visual observations during a run. For co-current upflow Specchia (1974) also identified three regimes using large (d_p = 0.6 cm) particles while Saada (1972) observed two regimes for smaller (d_p = 0.05–0.2 cm) particles. Our data were obtained in the bubble-flow region of Speccia and the single-phase pore flow region described by Saada. We observed identifiable gas bubbles rising through the continuous phase.

In the flow regimes of our study, k_sa and k_La do not differ greatly between cocurrent downflow, upflow or liquid-full (upflow). However, upflow leads to somewhat higher particle-to-liquid coefficients k_sa than downflow at high gas rates, low liquid rates, and smaller particle sizes. Upflow gives higher k_La than downflow at high gas and high liquid flow rates.

Nomenclature

a_t = total external surface area of particles per unit volume of empty tube, cm^2/cm^3
a = effective area for mass transfer, cm^2/cm^3
C = concentration, mol/cm^3
$C^*_{g,NA}$ = concentration of naphthalene in gas in equilibrium with saturated liquid
$C^*_{L,NA}$ = solubility of naphthalene in water, mol/cm^3
D = molecular diffusivity in liquid, cm^2/sec
d_p = particle diameter, cm
F_g = volumetric flow rate of gas at 1 atm, 25°C, cm^3/sec
F_L = volumetric flow rate of liquid at 1 atm, 25°C, cm^3/sec
H = Henry's law constant, C_g^*/C_L^*
J_D = mass transfer factor defined by eq 3
k_ga = gas-phase mass transfer coefficient in liquid-to-gas transport, $(sec)^{-1}$
k_La = liquid-phase mass transfer coefficient in liquid-to-gas transport, $(sec)^{-1}$
k_sa = liquid-phase mass transfer coefficient in particle-to-liquid transport, $(sec)^{-1}$
K_La, K_ga = overall mass transfer coefficients, $(sec)^{-1}$
Re_L = liquid-phase Reynolds number, $(D_p u_L \rho_L)/\mu_L$
S = cross-sectional area of empty tube, cm^2 (5.23 cm^2 for this work)
u_g = superficial velocity of gas, cm/sec
u_L = superficial velocity of liquid, cm/sec
$Y_{g,NA} = C_{g,NA}/C^*_{g,NA}$
$Y'_{g,NA} = C'_{g,NA}/C^*_{g,NA}$
z = packed bed depth; z_B = total depth of packing, cm

Greek Letters

ϵ_B = void fraction in the bed
ϵ_p = porosity in the particle
ρ_L = density of liquid, g/cm^3
ρ_p = apparent density of particle, g/cm^3
ρ_s = solid-phase density of particle, g/cm^3
μ_L = viscosity of liquid, g/(cm)(sec)

Subscripts

e = effluent from bed
f = feed to bed
g = gas phase
L = liquid phase
NA = naphthalene
O_2 = oxygen

Superscript

* = equilibrium condition
′ = denotes effluent from column with no packing

Literature Cited

Baldi, G., Goto, S., Chow, C. K., Smith, J. M., *Ind. Eng. Chem., Process Des. Dev.*, **13**, 447 (1974).
Evans, G. C., Gerald, C. F., *Chem. Eng. Prog.*, **49**, (3), 135 (1953).
Goto, S., Smith, J. M., *AIChE J.*, **21**, 706 (1975a).
Goto, S., Smith, J. M., *AIChE J.*, **21**, 714 (1975b).
Hirose, T., Toda, M., Sato, Y., *J. Chem. Eng. Jpn.*, **7**, 187 (1974).
Perry, J. H., "Chemical Engineer's Handbook," 4th ed, p 14-6, McGraw-Hill, New York, N.Y., 1963.
Reid, R. C., Sherwood, T. K., "The Properties of Gases and Liquids," 2nd ed, p 559, McGraw-Hill, New York, N.Y., 1966.
Saada, M. Y., *Chim. Ind. Gen. Chim.*, **105**, 1415 (1972).
Seidell, A., "Solubilities of Organic Compounds," 3rd ed, Vol. II, p 647, Van Nostrand, New York, N.Y., 1941.
Shulman, H. L., Robinson, R. G., *AIChE J.*, **6**, 469 (1960).
Snider, J. W., Perona, J. J., *AIChE J.*, **20**, 1172 (1974).
Specchia, V., Sicardi, S., Gianetto, A., *AIChE J.*, **20**, 646 (1974).
Van Krevelen, D. W., Krekels, J. T. C., *Recl. Trav. Chim.*, **67**, 512 (1948).
Washburn, E. W., Ed., "International Critical Tables," 1st ed, Vol. 3, p 208, McGraw-Hill, New York, N.Y., 1929.
Weekman, V. W., Myers, J. E., *AIChE J.*, **10**, 951 (1964).
Wilson, E. J., Geankoplis, C. J., *Ind. Eng. Chem., Fundam.*, **5**, 9 (1966).

Received for review February 24, 1975
Accepted June 10, 1975

The financial assistance of the Water Resources Center, University of California, Grant W-392, is gratefully acknowledged.